Supplement of Weather Clim. Dynam., 3, 449–469, 2022
https://doi.org/10.5194/wcd-3-449-2022-supplement
© Author(s) 2022. CC BY 4.0 License.

Supplement of

Circumglobal Rossby wave patterns during boreal winter highlighted by space–time spectral analysis

Jacopo Riboldi et al.

Correspondence to: Jacopo Riboldi (jacopo.riboldi@geo.uu.se)

The copyright of individual parts of the supplement might differ from the article licence.

Text S1: Description of the interpolation procedure

The interpolation of wavenumber/phase speed periodograms along lines of constant phase speed follows the approach documented by Randel and Held (1991). According to the Rossby wave dispersion relationship, points with constant phase speed have a constant ratio between frequency and wavenumber and appear, therefore, as tilted lines starting from the origin in the wavenumber/frequency periodogram.

Interpolation is linear in frequency and follows this series of steps:

1. Using the Rossby wave dispersion relationship the corresponding $\boldsymbol{\omega}^*$ is found for a given $\boldsymbol{c_p}$ and $\boldsymbol{n}^*$ at a given latitude.
2. The closest frequencies obtainable from the available 6-hourly resolution (converted in s-1) are found. Let us name them $\boldsymbol{\omega_l}$ and $\boldsymbol{\omega_h}$, with $\boldsymbol{\omega_l < \omega^* < \omega_h}$, and define the positive distances $\boldsymbol{\Delta\omega_l = \omega^* - \omega_l}$, $\boldsymbol{\Delta\omega_h = \omega_h - \omega^*}$ and $\boldsymbol{\Delta\omega = \omega_h - \omega_l}$.
3. A linear interpolation in frequency is performed to obtain the periodogram $\boldsymbol{P(n^*, c_p)}$ in the wavenumber/phase speed domain from the values $\boldsymbol{P(n^*, \omega_l)}$ and $\boldsymbol{P(n^*, \omega_t)}$ available in the wavenumber/frequency periodogram:

$$\boldsymbol{P(n^*, c_p) = \left[P(n^*, \omega_l) \cdot \left(1 - \frac{\Delta\omega_l}{\Delta\omega}\right) + P(n^*, \omega_t) \cdot \frac{\Delta\omega_t}{\Delta\omega}\right]}$$

A specular procedure is applied for negative frequencies to consider harmonics with $c_p < 0$.

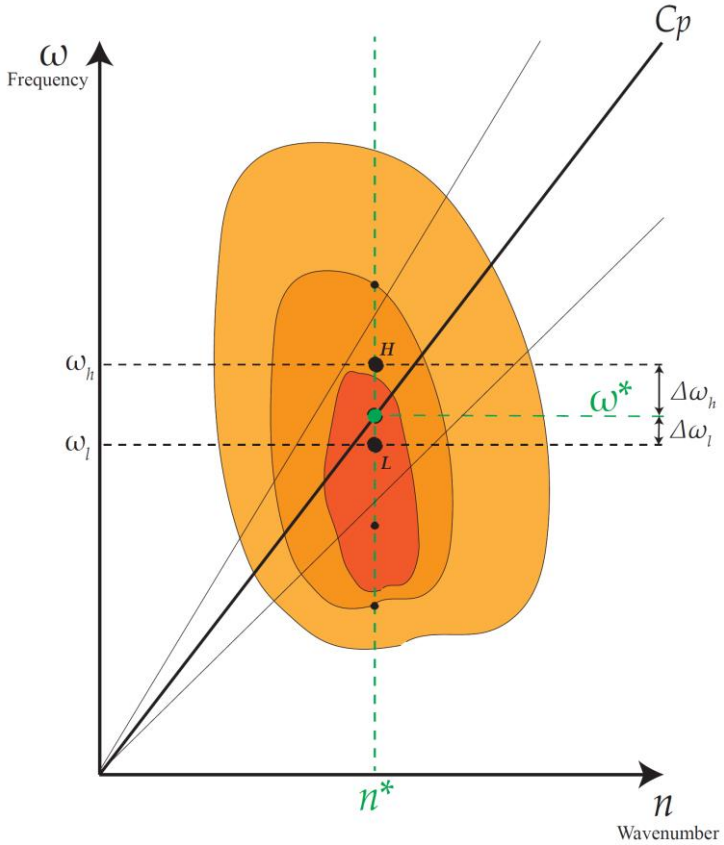

Fig. S1: Schematic showing a sketched wavenumber/frequency periodogram, with different colors indicating different values. Different symbols are explained in Text S1. Lines of constant phase speed are starting from the origin and have different tilt according to their magnitude.

Text S2: About unresolved wavenumber/phase speed harmonics

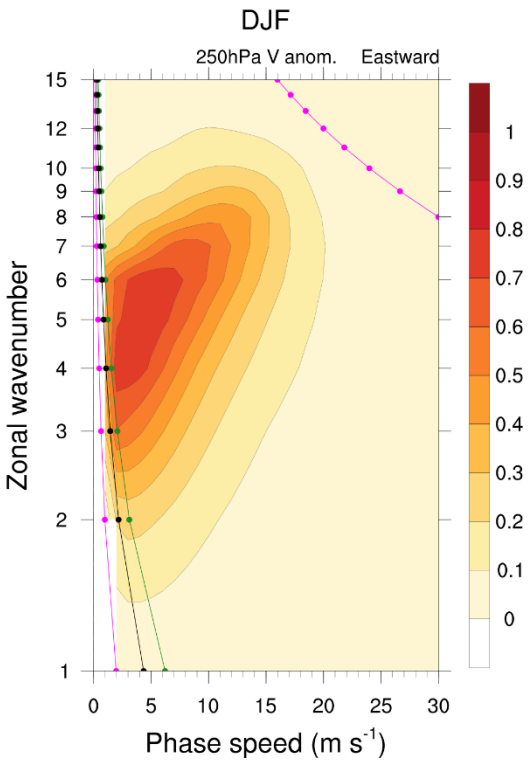

Fig. S2: Section of Fig. 1a depicting the climatological spectral power density for positive phase speed in DJF. Unresolved values of c_{min} for each wavenumber are overlaid for three different latitude circles: 35°N (green line), 55°N (black line) and 75°N (magenta line). Unresolved c_{max} are shown only for 75°N.

The time resolution of the data and the width of the time window chosen for the spectral analysis constrain the wavenumber/phase speed harmonics that is possible to resolve. This fact was already discussed by Randel and Held (1991), who indeed indicate with missing values such unresolved harmonics (cf. their Fig. 1b). Given that

$$c_p = \frac{\omega a cos\phi}{n},$$

the smallest values of c_p that is possible to resolve (c_{min}) are the ones corresponding to $\omega_{min} = \frac{2\pi}{61d}$, for each a-dimensional wavenumber n and latitude ϕ (as usual, a = 6371000 m). Analogously, the highest resolvable c_p value (c_{max}) corresponds to the highest resolved angular frequency, which is the Nyquist frequency $\omega_{max} = \frac{2\pi}{2 \cdot 6h}$.

The $cos\phi$ term in the definition of c_p implies that c_{min} decreases as latitude increases: this dependence upon latitude is shown in Fig. S2, where c_{min} is plotted for three different latitudes. The values of c_{min} for the first 8 zonal wavenumbers are tabulated here on the right. In the study we use a higher time resolution (6h vs daily) and a smaller time window (61d vs 121d) than Randel and Held (1991), improving the capability to resolve rapidly moving waves but reducing at the same time the capability to resolve slow-moving ones. Summing together the periodograms from different latitude circles allows to obtain information about harmonics that would otherwise remain unresolved. This implies, however, that for a few harmonics with particularly low wavenumber and phase speed the information comes predominantly from Rossby waves propagating at high latitudes. On the other hand, the harmonics between the green line on the left and the magenta line on the right in Fig. S2 are the vast majority and are properly resolved across the entire latitude range considered in this study (35°N-75°N).

n	c_{min} [m s^{-1}]		
	35°N	**55°N**	**75°N**
1	6.22	4.36	1.97
2	3.11	2.18	0.98
3	2.07	1.45	0.66
4	1.56	1.09	0.49
5	1.24	0.87	0.39
6	1.04	0.73	0.33
7	0.89	0.62	0.28
8	0.78	0.54	0.25

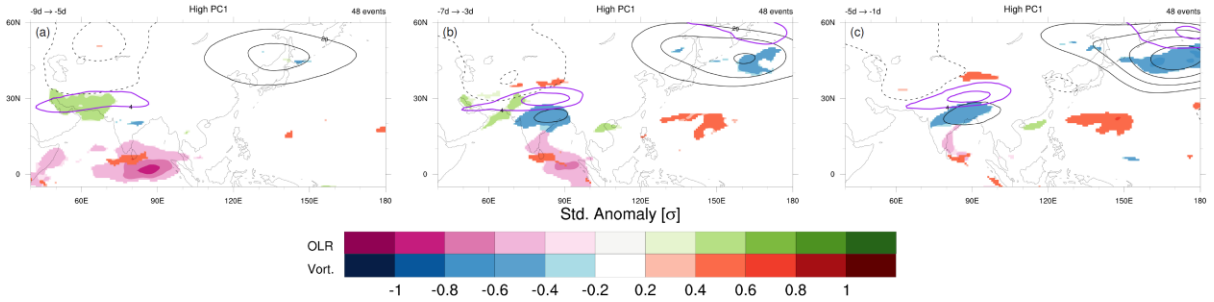

Fig. S3: Lagged composites of significant ($p<0.01$, two-sided t-test) pentad-mean standardized anomalies of OLR and 250hPa relative vorticity (shaded) for CRWP1 and events for the pentads centered at (a) t_{max} -7d (b) t_{max} -5d and (c) t_{max} -3d. Contours of pentad-mean 250hPa geopotential height anomalies (black contours, between -80m and +80m every 20m excluding zero) and positive 250hPa zonal wind anomalies (purple contours, only 4 m s^{-1} and 6 m s^{-1} isotachs) are overlaid.

Fig. S4(below): Lagged composites of significant ($p<0.01$, two-sided t-test) heptad-mean standardized anomalies of 775 hPa baroclinicity and 700 hPa transient meridional heat flux (shaded), together with heptad-mean geopotential height anomalies (brown contours, only -40m, +40m and +80m), for CRWP1 events. Standardized anomalies higher (lower) than +0.5σ (-0.5σ) are contoured by a bold continuous (dotted) black contour. All the heptads centered between t_{max}-6d and t_{max}+5d are shown. Averaging regions as in Fig. 9 in the manuscript.

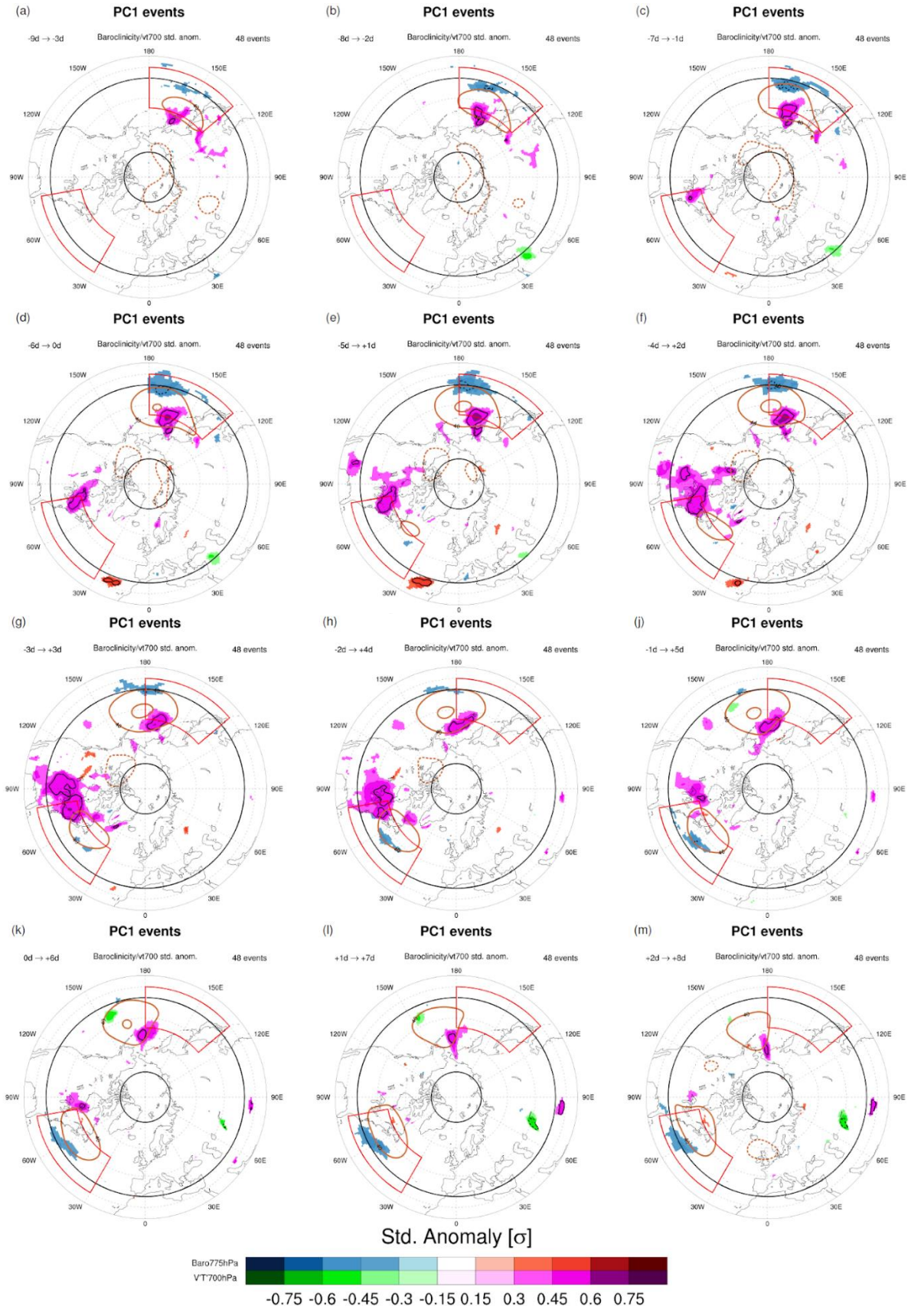
(a)
PC1 events
-9d → -3d
Baroclinicity/vt700 std. anom.
48 events
(b)
PC1 events
-8d → -2d
Baroclinicity/vt700 std. anom.
48 events
(c)
PC1 events
-7d → -1d
Baroclinicity/vt700 std. anom.
48 events
(d)
PC1 events
-6d → 0d
Baroclinicity/vt700 std. anom.
48 events
(e)
PC1 events
-5d → +1d
Baroclinicity/vt700 std. anom.
48 events
(f)
PC1 events
-4d → +2d
Baroclinicity/vt700 std. anom.
48 events
(g)
PC1 events
-3d → +3d
Baroclinicity/vt700 std. anom.
48 events
(h)
PC1 events
-2d → +4d
Baroclinicity/vt700 std. anom.
48 events
(j)
PC1 events
-1d → +5d
Baroclinicity/vt700 std. anom.
48 events
(k)
PC1 events
0d → +6d
Baroclinicity/vt700 std. anom.
48 events
(l)
PC1 events
+1d → +7d
Baroclinicity/vt700 std. anom.
48 events
(m)
PC1 events
+2d → +8d
Baroclinicity/vt700 std. anom.
48 events
180
150W
150E
120W
120E
90W
90E
60W
60E
30W
30E
0
Std. Anomaly [σ]
Baro775hPa
V'T'700hPa
-0.75 -0.6 -0.45 -0.3 -0.15 0.15 0.3 0.45 0.6 0.75

Table S1: CRWP1 events

# Event	Date of t_{max}	Duration [days]
1	1997-01-18	7
2	2005-01-16	10
3	1984-02-08	10
4	1983-01-12	36
5	2018-01-11	26
6	1988-01-27	15
7	1989-01-06	7
8	1990-02-23	14
9	2008-01-02	9
10	2004-12-25	10
11	2013-01-13	36
12	1990-12-23	20
13	1995-01-13	9
14	1996-12-18	15
15	1979-12-19	5
16	2011-02-14	8
17	1980-01-22	10
18	1994-12-19	5
19	2007-01-26	9
20	2017-12-06	9
21	2003-12-18	23
22	1983-12-14	6
23	1991-02-18	7
24	1982-01-19	19
25	1984-12-09	8
26	1998-02-21	8
27	1997-12-31	9
28	1996-02-20	11
29	2016-02-17	15
30	1980-12-01	9
31	1999-01-30	8
32	1997-12-11	6
33	1988-12-17	17
34	1982-12-03	6
35	2002-02-03	6
36	2005-02-03	14
37	1986-01-17	16
38	1994-02-19	9
39	1985-02-15	5
40	2017-02-28	15
41	2017-01-26	5
42	2010-12-11	11
43	2010-12-31	5
44	1989-02-23	5
45	1987-01-20	10
46	2015-12-18	5
47	2013-12-18	11
48	2014-12-29	9

Table S1: list of the 48 CRWP1 events used to compute composites, with the central date of the event (corresponding to the maximum in PC1) and the duration of the event in days.

Table S2: CRWP2 events

# Event	Date of t_{max}	Duration [days]
1	2019-01-23	46
2	1985-02-15	10
3	1987-02-10	8
4	2009-02-28	29
5	2016-02-15	23
6	1985-12-07	60
7	1994-01-05	11
8	2004-12-23	23
9	2018-01-05	9
10	1988-01-26	61
11	2015-02-19	6
12	2003-12-16	26
13	2015-01-05	23
14	1982-01-23	7
15	2001-02-02	17
16	1997-12-10	6
17	2014-02-15	5
18	2006-12-25	5
19	1994-02-07	15
20	1999-01-02	7
21	1993-12-01	14
22	2007-01-09	12
23	2006-01-15	14
24	1987-01-14	19
25	2002-01-23	5
26	2013-02-17	7
27	2013-12-19	5
28	2006-02-12	5
29	1999-12-05	10
30	2012-12-21	5
31	2018-01-25	9
32	1998-01-23	5
33	2001-01-01	11
34	1990-01-02	13
35	1985-01-22	11
36	2002-02-10	9
37	1995-02-21	5
38	2014-12-21	11
39	2007-02-19	8
40	2013-01-16	5
41	2011-12-03	11
42	1989-01-25	6

Table S2: list of the 42 CRWP2 events used to compute composites, with the central date of the event (corresponding to the maximum in PC2) and the duration of the event in days.